Proceedings of the Project Review, Geo-Mathematical Imaging Group (Purdue University, West Lafayette IN), Vol. 1 (2009) pp. 181-192.

SCALING OF DISPLACEMENT AND FLUID FLOW IN SINGLE FRACTURES

CHRISTOPHER L. PETROVITCH*, LAURA J. PYRAK-NOLTE†, AND DAVID D. NOLTE‡

Abstract. The relationship between the hydraulic and seismic properties of fractures is based on an empirical relationship between fluid flow through a fracture and fracture specific stiffness. Experimental work has shown that fracture stiffness and fluid flow through a fracture both depend on the topology of the fracture. In this study, we collapse the displacement-stress and flow-stress relationships using geometric length scales associated with the geometry of the fracture.

1. Introduction. Understanding the mechanical and hydraulic properties of single fractures is important in many scientific and engineering fields, i.e, nuclear waste isolation, oil & gas production, and carbon sequestration among others. Single fractures are composed of two rough surfaces in contact that results in a complicated distributions of void spaces, through which fluids flow, and areas of contact that provide mechanical stability. Cook [9] noted that the geometry of a single fracture primarily determines its mechanical deformation and hydraulic properties. This geometry has many length scales associated with it; for example the size and spatial distribution of the apertures (distance between the two rough surfaces or size of the voids) and contact areas. From a computational study, Pyrak-Nolte & Morris [20] surmised that the spatial correlation length of the aperture distribution in a single fracture is the defining length scale that affects the interrelationship between the hydraulic and mechanical response of a fracture. However, they did not fully explore which correlation length associated with the void geometry or contact is the most relevant length scale. For example, there are spatial correlation lengths associated with the percolation cluster (largest cluster of connected void space) and also with the separation between clusters. Both of these correlation lengths will be affected by changes in stress on a fracture because the void geometry and contact area are affected by stress. In this paper, we perform a computational study of the effect of fracture void geometry on both fluid flow and displacement of single fractures to determine the relevant length scales for future work on scaling the fluid flow-fracture specific stiffness relationship.

2. Fracture Model. There are many methods for generating fracture void geometry. Most numerical approaches for simulating synthetic fracture void geometry are based on generating two rough surfaces that are then brought into contact to form the void geometry (Pietgen & Saupe, [25]; Brown, [3]; Glover et al., [15]; Borodich & Onishchenko, [3]; Walsh et al., [32]). For example, Brown [4] developed a method for simulating fracture roughness by specifying the fractal dimension of the roughness, the root mean square roughness and a length describing the mismatch between the two fracture surfaces. In our approach, we use the stratified continuum percolation method to directly generate the void geometry of a fracture (i.e. the contact area and variable apertures voids) without generating two independent rough surfaces.

The stratified continuum percolation method (Nolte, [24]; Nolte & Pyrak-Nolte, [22, 23]) constructs a two-dimensional hierarchical aperture distribution with a tunable spatial correlation. The construction consists of generating self-similar cascades recursively. Each level in the recursion (tier) is a scaled-down random continuum percolation construction. Figure 1 shows an example of such a construction with two tiers, and 3 points per tier. The construction begins with a two dimensional array with each node equal to zero, i.e., the inital fracture is completely covered by contact area. The largest box is the first tier, and within it, three points were randomly chosen. These three points represent the center of the next tier (the next smaller sized boxes), which are scaled down by a scale factor, b. In each of the second tier boxes, three randomly located solid boxes or points are plotted. A point consists of a square composed of 4 pixels by 4 pixels. When a point is plotted in the array, each array element is incremented by one. The overlapping points result in an aperture

*Department of Physics, Purdue University, West Lafayette, IN 47907

†Department of Physics, Purdue University, West Lafayette, IN 47907, Department of Earth and Atmospheric Sciences, Purdue University, West Lafayette, IN 47907

‡Department of Physics, Purdue University, West Lafayette, IN 47907

distribution. This recursive approach leads to patterns with long-range spatial correlations because, as the tiers are scaled down, the area in which points are plotted is also reduced. The correlation length increases as tiers overlap, which is the case for the top two tiers in Figure 1.

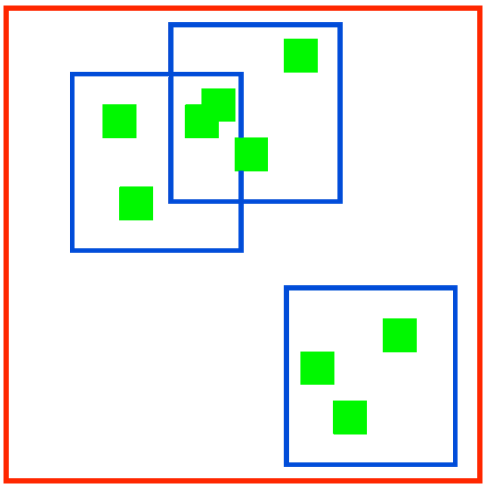

FIG. 1. *Example of how the stratified continuum percolation method generates fractures.*

In this study, two types of fractures (size 1024 pixels x 1024 pixels) were generated: (1) spatially uncorrelated fractures and (2) spatially correlated. The uncorrelated fractures were generated using one tier which is essentially standard random continuum percolation using 8000 - 200000 number of points per tier. The correlated fractures were generated using four tiers with a scale factor of b=4 and 10 - 38 points per tier. Examples are shown in Figure 2. The uncorrelated geometry acts as a control case with well defined percolation properties. By setting the scale factor to 4 for the correlated fractures, the percolation threshold approaches standard continuum percolation.

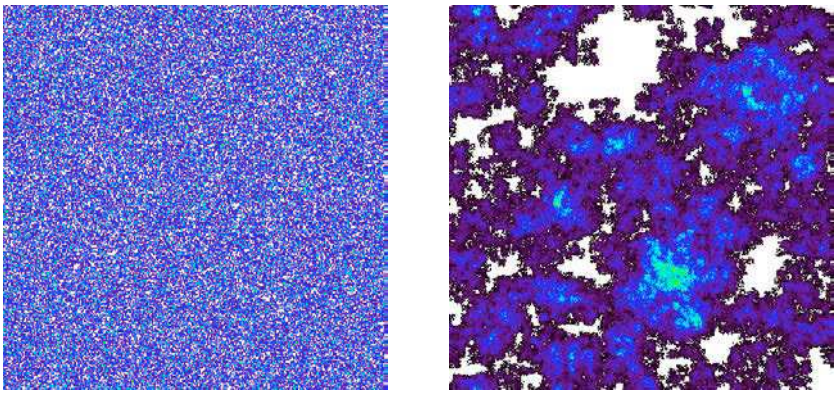

FIG. 2. *Example Fractures. White is contact (zero aperture) and Blue-Red represents increasing aperture. (a) Uncorrelated fracture with 1024 pixels on a side and* 10^5 *points per tier. (b) Correlated fracture with 1024 pixels on a side, 26 points per tier and scale factor of 4.*

3. Fracture Geometry. Pyrak-Nolte & Morris [20] noted the importance of fracture void geometry in linking the hydraulic and mechanical properties of a fracture. Thus, it is important to measure the relevant length scales of the simulated fractures. In standard 2D percolation, the parameter of the system that defines the critical point or percolation threshold [30] is the probability that any given site is occupied. It is not possible to use this parameter with stratified continuum

percolation because the plotted points are larger than the size of a pixel or one element in the array. In this study, a similar parameter is chosen: the fractional area of non-zero aperture of the pattern, A_f, i.e., the area of the void space.

In scaling studies, it is important to determine if a system is in the effective medium regime (far from threshold) or near threshold behavior. The scaling behaviors for these two regimes are different. For example, flow depends linearly on occupancy far from the percolation threshold, but near threshold exhibits a power law dependence (Cheng et al., [8]). We determined a threshold for both the mechanical and hydraulic behavior for our simulated fractures.

The threshold for the mechanical properties is intuitive. The mechanical threshold occurs when the void area covers the entire fracture, A_f=1. This is because stress is transmitted through the contact area of a fracture. As the area fraction approaches unity, any stress applied to the system acts on fewer and fewer regions of contact. At the limit when $A_f = 1$, the fracture is completely open with no points of contact and thus unable to transmit stress.

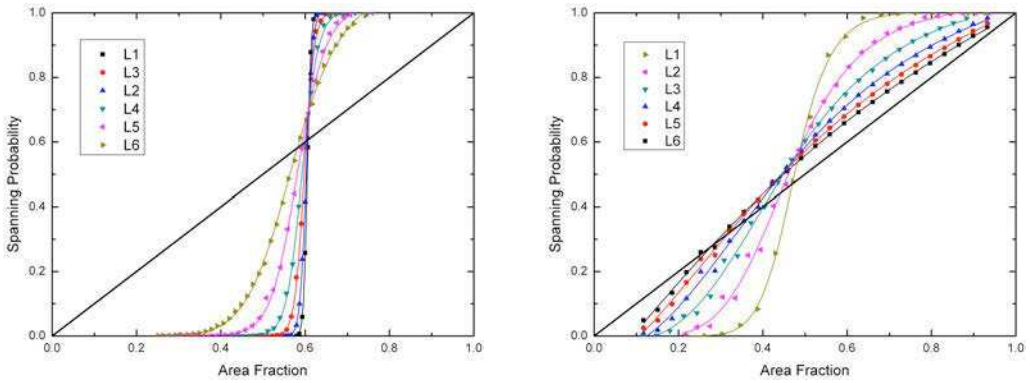

FIG. 3. *Probability that a spanning cluster exists as a function of area fraction. (a) Spanning probability of uncorrelated patterns. (b) Spanning probability of correlated patterns.*

The threshold for the hydraulic properties of a fracture are more complicated. Methods from 2D percolation theory are used to determine the hydraulic threshold because flow is dominated by the critical cluster of void volume of a fracture (i.e., the largest cluster of void space that spans the entire pattern),. The percolation threshold is determined from a graph of the probability that a spanning cluster exists as a function of area fraction. In the infinite limit, this function is a Heaviside step function centered at the threshold [30]. Because it is not possible to generate an infinite sized fracture, we use a renormalization group formalism to extrapolate our computational data to the infinite limit. In Figure 3, the spanning probability of the simulated fractures is shown for the largest fracture generated (L1) along with five smaller scales (L2=1/2; L3=1/4; L4=1/8; L5 = 1/16; L6=1/32). The smaller scales were generated by taking subsections of the original pattern (L1). The spanning probability is a function of the scale of the fracture. The probability that a spanning cluster exists across a fracture increases with decreasing size below the percolation threshold, while above threshold the spanning probability decreases with decreasing size. To determine the critical area fraction at the percolation threshold, each curve was fit with an incomplete beta function (Eq. 3.1).

$$B(x;\alpha,\beta) = \int_0^x t^{\alpha-1}\,(1-t)^{\beta-1}\,dt \tag{3.1}$$

The area fraction at which each curve intersects with the line $y = x$ defines a length, p*. By graphing, p* as a function of length scale (raised to the negative inverse of the critical exponent) of the fracture enables the extrapolation to the infinite limit, see Figure 4. The critical area fraction

for the uncorrelated fractures is approximately 0.609. The extrapolation in the case of correlated fractures requires some thought. It is known that the threshold for continuum percolation is 0.5. As Figure 4 shows, the values of p* increase monotonically toward one half. If one extrapolates using the largest scales (those least effected by finite size effects) the percolation threshold matches that of continuum percolation. This places the threshold at approximately 0.5.

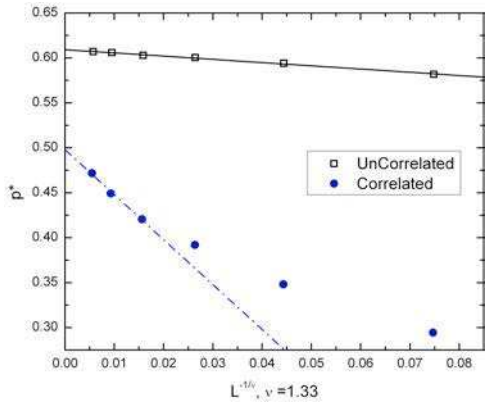

FIG. 4. *Extrapolation of p* to the infinite limit.*

The next step in understanding the fracture model is to investigate the different length scales of the fracture geometry. Four different correlation lengths are considered. Here percolation, geometric, separation and cluster correlation length. The percolation correlation length is the same correlation length used in traditional 2D percolation, i.e., the correlation length of the largest cluster. This is calculated from an autocorrelation analysis (Eq. 3.2) of the largest clusters, and the resulting autocorrelation function is fit with an exponential. The decay constant is taken to be the percolation correlation length. The geometric correlation length is the decay length of an exponential fit to the autocorrelation function for the entire void geometry, Eq. 3.2. The separation correlation length is similar to both the percolation and geometric lengths but is used to quantify the distance between clusters. Equation 3.3 gives the mathematical form of the separation correlation length, where α and β are cluster labels. By performing an autocorrelation analysis that excludes points within the same cluster, we are in essence calculating the average distance between clusters rather than the size of the clusters. Finally, the cluster correlation length scale considered in this study is the average cluster size. This is calculated by using Eq. 3.4, where α and β are, again, cluster labels. Converse to the separation correlation length, this analysis only auto-correlates regions that are contained within a cluster. This results in something similar to the autocorrelation 3.2, but enables the measurement of the average cluster size. Figure 5 illustrates the effect area fraction has on these length scales for both correlated and uncorrelated fractures. The geometric, percolation, and cluster correlation lengths both increase with increasing area fraction. The separation correlation length achieve a maximum value at the percolation threshold.

$$S(x,y) = \frac{1}{A}\int_A f(u,v)f(x+u,y+v)dudv \tag{3.2}$$

$$S_{sep}(x,y) = \frac{1}{A}\int_A (1-\delta_{\alpha\beta})\, f_\alpha(u,v)f_\beta(x+u,y+v)dudv \tag{3.3}$$

$$S_{cluster}(x,y) = \frac{1}{A}\int_A \delta_{\alpha\beta} f_\alpha(u,v)f_\beta(x+u,y+v)dudv \tag{3.4}$$

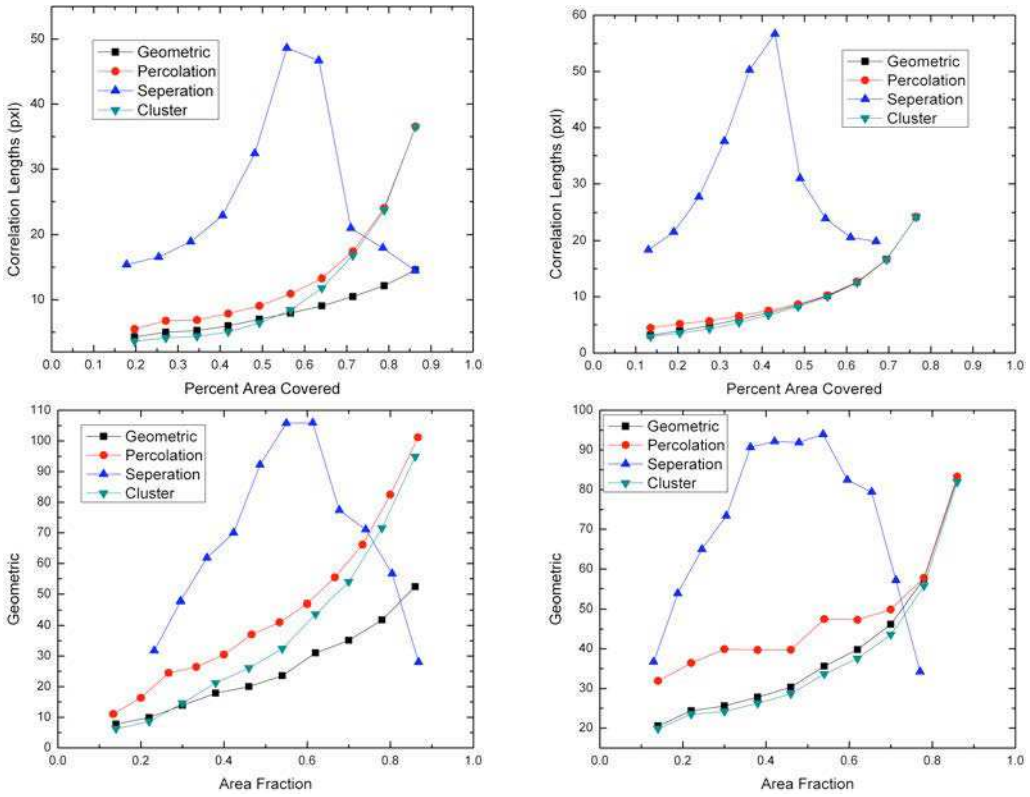

FIG. 5. *Four different correlation lengths as a function of area fraction. Fractures were generated with a edge length of 256 pixels. (a) Uncorrelated void area is analyzed. (b) Uncorrelated contact area is analyzed. (c) Correlated void area is analyzed. (d) Correlated contact spaces are analyzed.*

4. Deformation Model. To investigate the relationship between the mechanical and hydraulic properties of fractures, it is necessary to calculate the deformation of a fracture when subjected to a normal load. In this study, fractures were deformed numerically under a normal load using a method similar to Hopkins' [10]. Prior to Hopkins [10], most approaches for deforming a fracture assumed a uniform deformation for the solid matrix material or allowed interpenetration of the asperities,(Greenwood & Williamson, [17]; Gangi, [14]; Brown, [26]). Unlike those approaches, Hopkins' [10] model included interaction among the asperities and the related deformation of the solid matrix. Pyrak-Nolte & Morris [20] decreased the computational load of Hopkins' original algorithm by solving the required system of linear equations more efficiently.

The fracture deformation is calculated by assuming a joint can be modeled by two parallel half-spaces separated by an aperture distribution. Each asperity is modeled as a right cylinder arranged on a regular lattice. The height of the cylinders are determined from the fracture generation model and are given a radius such that all cylinders initially are in contact with neighboring cylinders (Figure 6a). For our study, the cylinders were given a radius, a, so that the largest fractures deformed were 1m x 1m on a side or a=0.48mm. We also assumed the physical properties of granite: Young's modulus = 60.0 GPa and Poisson's ratio = 0.25.

In Hopkins' model [10], the half-spaces and asperities are allowed to deform elastically under a normal load. It has been shown that the half-space's normal displacement under a uniformly loaded circle (normal to the half-space) is given by [29]:

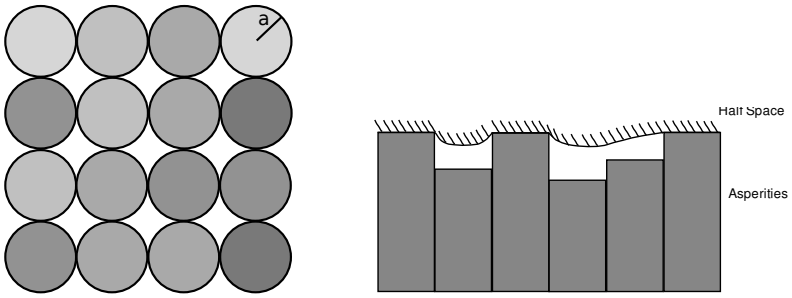

FIG. 6. *Deformation Model. (a) The Deformation model aligns the standing cylinders along a lattice grid. The shades of gray represent different asperity heights. (b) This illustrates the half-space deforming around the asperities as well as the asperities deformation.*

$$w_0 = f\frac{4\left(1-\nu^2\right)}{\pi^2 Ea}\left(\frac{r}{a}\right)\times\left[\int_0^{\frac{\pi}{2}}\sqrt{1-(a/r)^2\sin^2\theta}d\theta-\left[1-\frac{a^2}{r^2}\right]\int_0^{\frac{\pi}{2}}\frac{d\theta}{\sqrt{1-(a/r)^2\sin^2\theta}}\right] \tag{4.1}$$

ν = Poisson's ratio
E = Young's modulus
a = radius of the asperity
r = the distance from the center of the asperity
f = force acting on the asperity

From this, the average displacement over the entire fracture is calculated, which is similar to the displacement measured in the laboratory. The average displacement is determined by finding the total displacement at each asperity (i) (Eq. 4.2) and dividing it by the area of the interacting asperity (j), see Eq. 4.3.

$$d_{ij} = \iint_A w_0 dr d\theta \tag{4.2}$$

$$\bar{d}_{ij} = \frac{d_{ij}}{\pi a^2} \tag{4.3}$$

The equations above assume that $i \neq j$. The equation used to calculate the self interaction between the half-space and asperity ($i = j$) is:

$$\bar{d}_{ii} = f_i\frac{8\left(1-\nu^2\right)}{\pi^2 Ea}\iint_A\sqrt{1-(a^2/r^2)\sin^2\theta}dr d\theta \tag{4.4}$$

The total displacement at an asperity (i) caused by the deformation of all of the other asperities is,

$$W_i = \sum_{j\in C}\bar{d}_{ij} \tag{4.5}$$

where C is the set of asperities in contact. At this point in the analysis, the displacements at asperity (i) are specified and the compression of the asperity is,

$$\Delta h_i = \frac{f_i h_i}{\pi a^2 E} \tag{4.6}$$

where h_i is the initial height of asperity (i). The force exerted by a given asperity depends on the displacement of the half-spaces. Yet the displacement of the half-spaces depends on the forces exerted by all of the other asperities. This is converted into a linear system of equations by noting that the initial sum of the distances between the half-spaces, D, and the total deformation, W_i, must be equal to the length of the asperity, or

$$D + W_i = h_i - \Delta h_i \tag{4.7}$$

Because W_i depends indirectly on Δh_i through Eq. 4.6, Eq. 4.7 is a system of simultaneous linear equations in terms of Δh_i. This system is large ($N^2 \times N^2$, where N is the number of asperities in contact), non-sparse, and thus computationally intense to solve directly. Pyrak-Nolte and Morris [20] decreased the computational load by solving the system via the Conjugate-Gradient (CG) method, which reduces the system to a matrix-vector multiplication. The increased speed in computation comes from using the Fast Multipole method to increase the speed of the multiplication. This method capitalizes on the fact that long-range interactions are simple to compute with an approximation, whereas the short range interactions require full computation. The only issue with solving the system of equations in this manner is that the number of asperities in contact must be known before solving. This is handled by first solving the system and if any new asperities come into contact, resolving the system using the last solution as an initial guess in the CG method.

The fracture specific stiffness, κ, is calculated from the displacement-stress curves generated by the deformation model. Stiffness is defined as

$$\kappa(\sigma) = \left(\frac{d\sigma}{d\delta}\right) \tag{4.8}$$

where σ is the stress applied to the fracture and δ is the average displacement of the fracture:

$$\delta_i = \begin{cases} D_0 - D - W_i & \text{if not in contact} \\ D_0 - h_i + \Delta h_i & \text{if in contact} \end{cases} \tag{4.9}$$

$$\delta = \sum_i \frac{\delta_i}{N} \tag{4.10}$$

where D_0 is the zero-stress spacing between the half-spaces.

5. Fluid Model. A fluid-flow model is required to investigate the relationship between the mechanical and hydraulic properties of fractures. The flow properties of fractures were predicted numerically using a network model similar to that of Yang et al. [13, 12], Tran [18], and Cheng et al., [8]. In this model, the aperture distribution (or voids of the fracture) is replaced by a network of elliptical pipes beginning from the inlet side of the fracture to the outlet side. This differs from other models in that it is not direction blind, i.e. global flow and local flow are assumed to be in the same direction. Each row of aperture elements perpendicular to the flow is considered in turn, and large regions of non-zero apertures are brought together into a single large flow element. Between the rows, flow is calculated base on the analytic solution to flow in an elliptical pipe with conductances based on the apertures (see Tran [18] or Cheng, [7]). The model also assumes that the local flow is predominantly in the same direction of the main flow path by only allowing the paths (from row to row) to diverge 45 degrees or less. This model is preferred over the bi-lattice grid method, used in [20], because it is computationally more efficient (run times are 4-10 times faster) and it was shown to model 2D micro-model experimental data more accurately [8].

6. Fracture Stiffness and Fluid Flow simulations. Pyrak-Nolte [27] and Pyrak-Nolte & Morris [20] showed that fluid flow and fracture specific stiffness are related through the geometry of the fracture, specifically the size and spatial distributions of aperture and contact area. This is an important relationship because fracture specific stiffness can be determined from seismic wave attenuation and velocity (Pyrak-Nolte et al., [28], Lubbe et al., [21], Worthington, [33]), thus potentially

enabling the link between seismic measurements and the hydraulic properties of fractures. These previous studies did not try to determine which spatial correlation lengths affect this relationship or whether a scaling relationship exists.

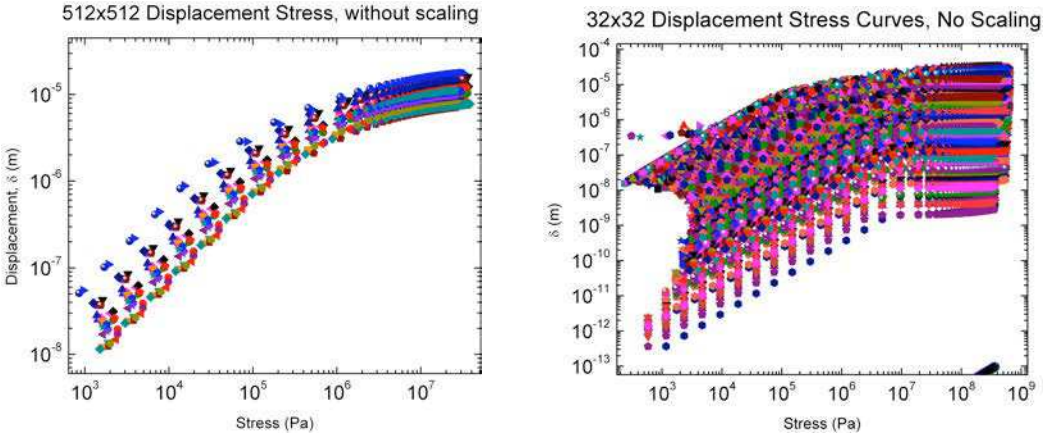

FIG. 7. *Displacement vs Stress curves for simulations of L2 (a) and L6 (b).*

In this study, eight correlated fractures were created using 4 tiers with a scale factor of 4 and 30 number of points per tier. To explore a scaling relationship between fluid flow and fracture specific stiffness, simulations were run on fractures of various sizes. Fractures were generated with an initial size of 1024 (L1) pixels on a side, and then subsections were taken with 512 (L2), 256 (L3), 128 (L4), 64 (L5), and 32 (L6) pixels on a side. Each fracture (as well as sub-fracture) was placed under a normal load. Fluid flow simulations were performed for each increment of stress. Unfortunately, the largest scale was computationally too intensive to deform, so this analysis only includes fractures of scales L2 to L6. The fractures were generated so that the area fractions at the L1 scale was approximately 0.75 to force the area fraction to fall between the mechanical threshold ($A_c = 1$) and the percolation threshold ($A_c = 0.5$). As the scale is decreased (i.e., sub-fractures are analyzed), the area fraction fluctuates because a sub-fracture may consist of all contact area, partial contact area or all void space. This fluctuation in void area increases the dispersion in the displacement and flow curves, see Figures 7 and 8. Only the largest and smallest sub-fracture results are shown. Figures 7 and 8 are plots of the displacement of each fracture as a function of the applied normal load. Each curve is the displacement, Figure 7, and flow rate, Figure 8, of a different sub-fracture.

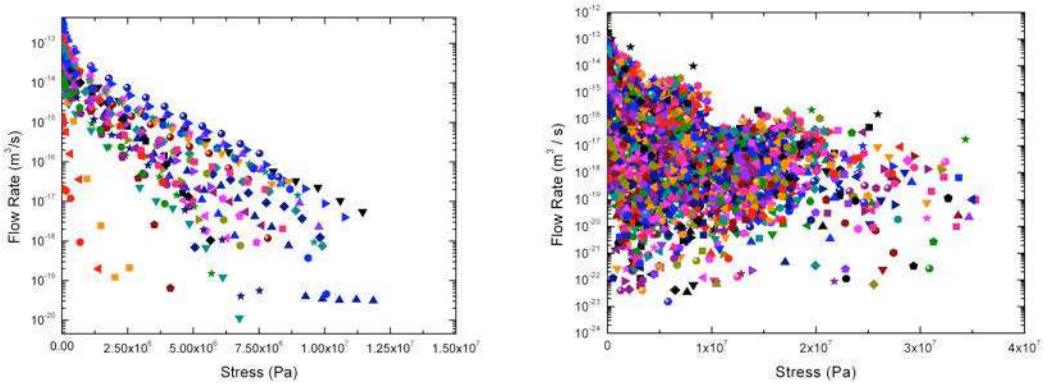

FIG. 8. *Flow vs Stress curves for simulations of L2 (a) and L6 (b).*

7. Data Collapse. In this paper, we perform a zeroth order collapse of the statistical fluctuation in the data. It has been shown that the contact area directly affects the displacement of a fracture under a normal load (Kendall & Tabor, [19]; Goodman, [16]; Swan, [31]; Bandis et al., [1]; Barton et al., [2]; Brown & Scholz, [5, 6]; Hopkins et al., [11, 10] ; Cook, [9]). This suggested that the displacement should be scaled by the contact area at each given stress. Also, because the maximum amount of displacement of a fracture is directly related to its void volume, we also scaled the displacement by the inverse of the volume. The results are shown in Figure 10. By comparing Figure 7 (a) & (b) with Figure 10 (a) & (e), the effect of normalizing the displacement by the ratio of initial void volume to contact area is observed. The normalized displacement as a function of stress almost collapses to a single curve. Additional analysis is needed to determine which correlation length(geometric, separation, cluster size) results in the remaining dispersion observed in the curves.

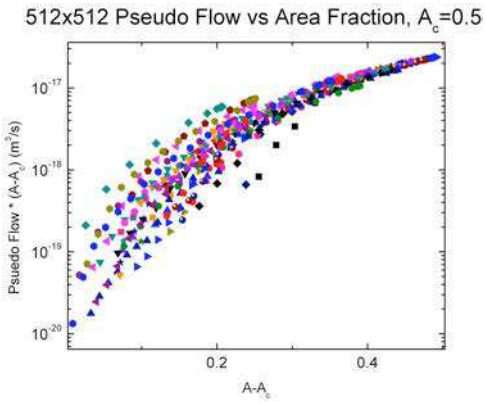

FIG. 9. *Scaled Flow curves for L2.*

To scale the flow curves as a function of stress, the system was treated as two dimensional flow, i.e., all non-zero apertures were set to unity. This approach enables us to determine the effect of the spatial correlations in void space on the flow-stress behavior because the dominant affect of aperture was removed. We used the standard scaling from 2D percolation theory that scales the flow by $(A_f - A_c)$ for each given area fraction, Figure 7. From this, it is observed that the flow behavior at high area fractions is in the effective medium regime ($A_f \gg A_c$) and moves into the critical regime as the percolation threshold, A_c, is approach. In the effective medium regime, all the curves are tightly packed or collapsed (Figure 9), and then diffuse as they approach the critical percolation threshold. Our ongoing research is to remove the dispersion as the percolation threshold is approached by incorporating the appropriate correlation lengths in our analysis.

8. Conclusions and Future Analysis. We have discussed our initial attempt to find a scaling relation between fluid flow and fracture displacement. Our work illustrates zeroth-order data collapse of displacement and flow as a function of stress. Our work suggests that the statistical fluctuations in the flow and displacement simulations can be partially collapsed based on the void volume of the fracture and contact area. This is an important first step before we attempt to analyze the universal scaling functions of both stiffness and flow as well as their relationship. Our next step is to attempt higher order collapses by incorporating the various correlation lengths discussed in section 2.

9. Acknowledgments. The authors wish to acknowledge Joe Morris for his assistance with code development. This work is supported by the Geosciences Research Program, Office of Basic Energy Sciences US Department of Energy (DEFG02-97ER14785 08) and is funded in part by the Geo-mathematical Imaging Group at Purdue University.

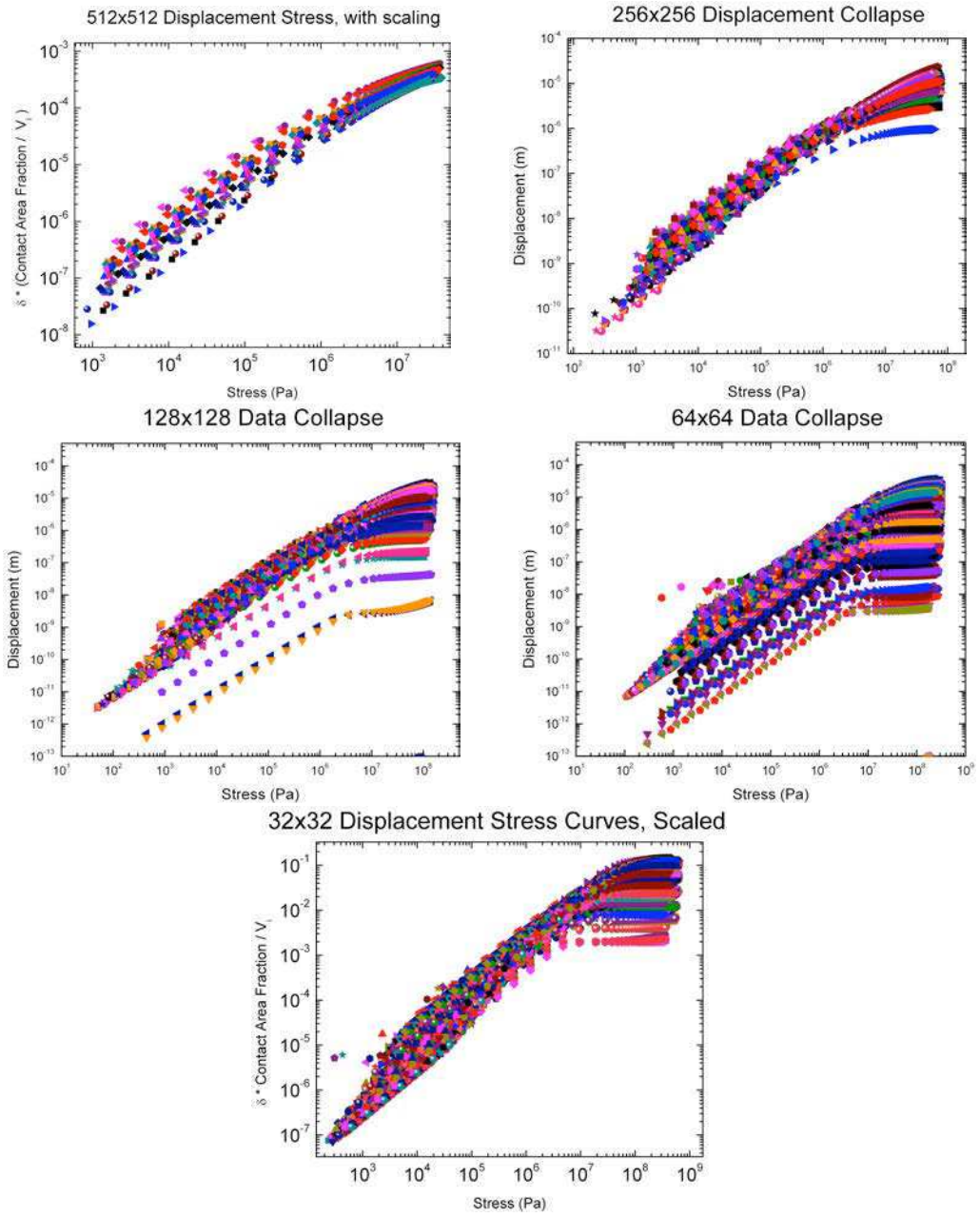

FIG. 10. *Scaled displacement-stress curves for simulations of L2 - L6 ((a) - (e) respectively).*

REFERENCES

[1] SC Bandis, AC Lumsden, and NR Barton. Fundamentals of rock joint deformation. *International Journal Of Rock Mechanics And Mining Sciences*, 20(6):249–268, 1983.

[2] N Barton, S Bandis, and K Bakhtar. Strength, Deformation And Conductivity Coupling Of Rock Joints. *International Journal Of Rock Mechanics And Mining Sciences*, 22(3):121–140, 1985.

[3] FM Borodich and DA Onishchenko. Similarity and fractality in the modelling of roughness by a multilevel profile with hierarchical structure. *International Journal of Solids and Structures*, 36(17):2585–2612, Jun 1999.

[4] SR Brown. Simple methematical-model of a rough fracture. *Journal of Geophysical Research-solid Earth*,

100(B4):5941–5952, APR 10 1995.

[5] SR Brown and CH Scholz. Closure Of Random Elastic Surfaces In Contact. *Journal Of Geophysical Research-Solid Earth And Planets*, 90(NB7):5531–5545, 1985.

[6] SR Brown and CH Scholz. Closure of rock joints. *Journal Of Geophysical Research-Solid Earth And Planets*, 91(B5):4939–4948, APR 10 1986.

[7] JT Cheng and N Giordano. Fluid flow through nanometer-scale channels. *Physical Review E*, 65(3, Part 1), Mar 2002.

[8] J.T. Cheng, J.P. Morris, J. Tran, A. Lumsbaine, N.J. Giordano, D.D. Nolte, and L.J. Pyrak-Nolte. Single-phase flow in a rock fracture: micro-model experiments and network flow simulation. *International Journal of Rock Mechanics and Mining Sciences*, 41:687–693, 2004.

[9] NGW Cook. Natural joints in rock: Mechanical, hydraulic, and seismic properties under normal stress. *Int J of Rock Mech Min Sci and Geomech Abstr*, pages 198–223, 1992.

[10] Hopkins D.L. *The Effect of Surface Roughness on Joint Stiffness, Aperture, and Acustic Wave Propagation*. PhD thesis, University of California at Berkeley, 1990.

[11] Hopkins DL, Cook NGW, and Myer LR. Fracture stiffness and aperture as a function of applied stress and contact geometry. In *Rock Mechanics: Proceedings of the 28th US Symposium*, pages 81–88, 1994.

[12] Yang G, Myer LR, Brown SR, and Cook NGW. Microscopic analysis of macroscopic transport-properties of single natural fractures using graph-theory algorithms. *Geophys Res Lett*, 1995.

[13] Yang G, Cook NGW, and Myer LR. Network modelling of flow in natural fractures as a guide for efficient utilization of natural resources. *Proceedings of 30th US Symposium on Rock Mechanics*, pages 57–64, 1989.

[14] AF Gangi. The variation of mechanical and transport properties of cracked rock with pressure. *Proceedings of 22th US Symposium on Rock Mechanics*, 1981.

[15] PWJ Glover, K Matsuki, and K Hayashi. Synthetic rough fractures in rock. *Journal of Geophysics Research - Solid Earth*, 103:9609–9620, 1998.

[16] RE Goodman. *Methods of geological engineering in discontinuous rocks*. St. Paul: West Pub. Co., 1976.

[17] JA Greenwood and JB Williamson. Contact Of Nominally Flat Surfaces. *Proceedings Of The Royal Society Of London Series A-Mathematical And Physical Sciences*, 295, 1966.

[18] Tran JJ. Efficient simulation of multiphase flow in three-dimensional fracture netowrks. Master's thesis, Department of Computer Science and Enginnering, Notre Dame University, 1998.

[19] K Kendall and D Tabor. Ultrasonic study of area of contact between stationary and sliding surfaces. *Proceedings of the Royal Society of London series A-Mathematical and Physical Sciences*, 323(1554), 1971.

[20] Pyrak-Nolte LJ and Morris JP. Single fractures under normal stress: The relation between fracture stiffness and fluid flow. *International Journal of Rock Mechanics and Mining Sciences*, 37:245–262, 2000.

[21] R. Lubbe, J. Sothcott, M. H. Worthington, and C. Mccann. Laboratory Estimates Of Normal And Shear Fracture Compliance. *Geophysical Prospecting*, 56(2):239–247, Mar 2008.

[22] DD Nolte and LJ Pyrak-Nolte. Stratified continuum percolation - scaling geoemetry of hierarchical cascades. *Physical Review A*, 44(10):6320–6333, Nov 15 1991.

[23] DD Nolte and LJ Pyrak-Nolte. Coexisting two-phase flow in correlated two-dimensional percolation. *Physical Review E*, 56(5, Part A):5009–5012, NOV 1997.

[24] DD Nolte, LJ Pyrak-Nolte, and NGW Cook. The fractal geometry of flow paths in natural fractures in rock and the approach to percolation. *Pure and Applied Geophysics*, 131(1-2):111–138, 1989.

[25] H. Peitgen and D. Saupe. *The science of fractal images*. Springer, 1988.

[26] WL Power, TE Tullis, SR Brown, GN Boitnott, and CH Scholz. Roughness of natural fault surfaces. *Geophysical Research Letters*, 14(1):29–32, JAN 1987.

[27] LJ Pyrak-Nolte and CD Montemagno. The effect of the critical path on fluid-flow through a fracture. In *Rock Mechanics: Models and Measurements challenges from Industry*, pages 81–88, 1994.

[28] LJ Pyrak-Nolte, LR Myer, and NGW Cook. Transmission Of Seismic-Waves Across Single Natural Fractures. *Journal Of Geophysical Research-Solid Earth And Planets*, 95(B6):8617–8638, Jun 10 1990.

[29] Timoshenko SP and Goodier JN. *Theory of elasticity 3rd ed.* McGraw-Hill, 1970.

[30] Dietrich Stauffer and Amnon Aharony. *Introduction to Percolation Theory*. CRC Press, 1985.

[31] G Swan. Determination of stiffness and other joint properties from roughness measurements. *Rock Mechanics and Rock Engineering*, 16(1):19–38, 1983.

[32] R. Walsh, C. McDermott, and O. Kolditz. Numerical modeling of stress-permeability coupling in rough fractures. *Hydrogeology Journal*, 16:613–627, 2008.

[33] M. H. Worthington and R. Lubbe. The Scaling Of Fracture Compliance. In Lonergan, L And Jolly, Rjh And Rawnsley, K And Sanderson, Dj, editor, *Fractured Reservoirs*, volume 270 of *Geological Society Special Publication*, pages 73–82, 2007.